1 **Genetically encoded sensors for measuring histamine release both *in vitro* and *in vivo***

2

3 Hui Dong[1,2,6], Mengyao Li[1,2,6], Yuqi Yan[1,2,3], Tongrui Qian[1,2], Yunzhi Lin[1,2], Xiaoyuan Ma[4], Henry

4 F. Vischer[4], Can Liu[1,2], Guochuan Li[1,2], Huan Wang[1,2], Rob Leurs[4], Yulong Li[1,2,3,5*]

5 [1] State Key Laboratory of Membrane Biology, Peking University School of Life Sciences, Beijing

6 100871, China.

7 [2] PKU-IDG/McGovern Institute for Brain Research, Beijing 100871, China.

8 [3] Peking-Tsinghua Center for Life Sciences, Academy for Advanced Interdisciplinary Studies,

9 Peking University, Beijing 100871, China

10 [4] Division of Medicinal Chemistry, Faculty of Science, Amsterdam Institute for Molecules,

11 Medicines and Systems, Vrije Universiteit Amsterdam, 1081 HZ Amsterdam, The Netherlands.

12 [5] National Biomedical Imaging Center, Peking University, Beijing, 100871, China.

13 [6] These authors contributed equally.

14 * Correspondence: yulongli@pku.edu.cn

15

16 **Abstract**

17 Histamine (HA) is a key biogenic monoamine involved in a wide range of physiological and

18 pathological processes in both the central nervous system and the periphery. Because the ability to

19 directly measure extracellular HA in real-time will provide important insights into the functional

20 role of HA in complex circuits under a variety of conditions, we developed a series of genetically

21 encoded G protein-coupled receptor activation-based (GRAB) HA (GRAB$_{HA}$) sensors. These

22 sensors produce a robust increase in fluorescence upon HA application, with good photostability,

23 sub-second kinetics, nanomolar affinity, and high specificity. Using these GRAB$_{HA}$ sensors, we

24 measured electrical stimulation-evoked HA release in acute brain slices with high spatiotemporal

25 resolution. Moreover, we recorded HA release in the preoptic area of the hypothalamus and in the

26 medial prefrontal cortex during the sleep-wake cycle in freely moving mice, finding distinct patterns

27 of HA release in these specific brain regions. Together, these *in vitro* and *in vivo* results show that

28 our GRAB$_{HA}$ sensors have high sensitivity and specificity for measuring extracellular HA, thus

29 providing a robust new set of tools for examining the role of HA signaling in both health and disease.

30

31 **Introduction**

32 The biogenic amine histamine (HA) is an important signaling molecule in the immune, digestive,

33 and nervous systems. For example, HA is secreted by basophils and mast cells as part of a localized

34 immune response, playing a role in allergy and itch[1]. HA is also released by enterochromaffin-like

35 cells in the stomach, triggering the release of stomach acids[2]. Since the discovery that antihistamines

36 also have sedative properties, the role of HA in the central nervous system has attracted considerable

37 attention[3]. In the vertebrate brain, HA is synthesized primarily in the tuberomammillary nucleus

38 (TMN) in the posterior hypothalamus[4], and histaminergic TMN neurons project throughout the

39 brain, regulating various functions such as the sleep-wake cycle, feeding, attention, and learning[5].

40   Despite its clearly important role in a wide range of physiological and pathological processes,

41 the spatiotemporal dynamics of HA release during various behaviors remain poorly understood, due

42 in large part to the limitations associated with current detection methods. For example, microdialysis

43 combined with analytical techniques has been widely used to measure the dynamics of HA release

44 in the living brain[6]. However, microdialysis often has low temporal resolution due to the relatively

45   long time needed to collect the samples. In addition, complementary approaches using
46   electrochemical methods such as fast-scan cyclic voltammetry have been developed for detecting
47   HA in real time[7]. However, both microdialysis and electrochemical methods have limited spatial
48   precision and lack cell-type specificity. Coupling diamine oxidase with an optical oxygen
49   nanosensor can provide continuous tracking of HA concentration[8], but the nanosensor has low
50   sensitivity (with a lower limit of detection of approximately 1.1 mM) and specificity, and is less
51   effective at detecting HA in deep brain regions. The Tango-Trace strategy can be used to detect HA
52   release *in vivo* with a high signal-to-background ratio by coupling the β-arrestin signaling pathway
53   to the expression of a reporter gene[9-11]. However, this approach requires several hours to express the
54   fluorescent reporter protein and cannot be used to monitor the rapid dynamics of HA-mediated
55   transmission. Finally, conformational H_1R and H_3R sensors based on both fluorescence resonance
56   energy transfer (FRET) and bioluminescence resonance energy transfer (BRET) have been
57   developed to measure their interaction with histamine (and mechanical force or other H_3R ligands,
58   respectively)[12-14], but generally have a low signal-to-noise ratio and a low dynamic range, thus
59   strongly limiting their ability to monitor HA release *in vivo*.

60   Recently, building on the successful G protein-coupled receptor activation–based (GRAB)
61   strategy, our group and others independently developed a series of genetically encoded sensors for
62   detecting a variety of neurotransmitters and neuromodulators with high sensitivity, selectivity, and
63   spatiotemporal resolution in *in vivo* preparations[15-19]. Using this strategy, we developed a pair of
64   genetically encoded fluorescent sensors called $GRAB_{HA1h}$ and $GRAB_{HA1m}$ (abbreviated here as
65   HA1h and HA1m, respectively) based on the human H_4R and water bear (tardigrade) H_1R receptors,
66   respectively, in order to measure extracellular HA with high sensitivity and high spatiotemporal
67   resolution both *in vitro* and *in vivo*. These sensors have high specificity for HA, rapid kinetics (on
68   the order of sub-second), and an increase in fluorescence of approximately 300-500% in response
69   to HA when applied *in vitro*. Using these novel HA sensors, we monitored the release of endogenous
70   HA during the sleep-wake cycle in freely moving mice and found distinct patterns of HA release in
71   two specific brain regions. Thus, these genetically encoded sensors can be used to gain important
72   new insights into the dynamic properties of HA signaling under both physiological and pathological
73   conditions.

74

75   **Results**
76   **Development and characterization of GRAB sensors for detecting histamine**
77   To monitor the change in extracellular HA levels with high spatial and temporal resolution, we
78   designed a genetically encoded GRAB sensor based on HA receptors (Fig. 1a). First, we
79   systematically screened a series of G protein-coupled HA receptors, including human H_1R, H_2R,
80   H_3R, and H_4R (Supplementary Fig. 1a,b). The third intracellular loop (ICL3) in the HA receptors
81   was replaced with a circularly permutated EGFP (cpEGFP) and ICL3 derived from the previously
82   developed and characterized $GRAB_{NE}$ norepinephrine sensor[20]. We selected the hH_4R-based
83   chimera, which has good plasma membrane trafficking (Supplementary Fig. 1b), for further
84   optimization. We then optimized the length and amino acid composition of the linker region near
85   the insertion site, as well as critical residues in cpEGFP based on our previous experience in
86   developing GRAB sensors (Fig. 1b). Screening more than 2,000 sensor variants resulted in the
87   sensor with the highest fluorescence response, which we called HA1h (Fig. 1b, Supplementary Fig.
88   2a). When expressed in cultured HEK293T cells, HA1h trafficked to the plasma membrane and

89 produced a peak change in fluorescence ($\Delta F/F_0$) of ~370% in response to extracellular application
90 of 10 μM HA (Fig. 1f-i). We also generated an HA-insensitive form of this sensor, which we call
91 HA1mut, by introducing an E211A substitution in hH_4R (Fig. 1b, Supplementary Fig. 2a). HA
92 application induced a dose-dependent increase in fluorescence in HA1h-expressing HEK293T cells,
93 with a half-maximal effective concentration (EC50) of 17 nM (Fig. 1j). Consistently, a similar
94 binding affinity (K_d) of 13 nM was obtained for the binding of [^{3}H]HA to HA1h in a radioligand
95 binding assay (Supplementary Fig. 5a). We also sought to develop a more sensitive HA sensor with
96 a higher response and a larger dynamic range by screening HA receptors obtained from 11 species
97 in which we grafted the ICL3-cpEGFP module from the HA1h sensor (Fig. 1c,d). Based on the
98 results of this screen, we selected the sensor based on the water bear (tardigrade) H_1R for further
99 optimization, yielding a high-response sensor we call HA1m (Fig. 1e, Supplementary Fig. 2b),
100 which produces an ~590% increase in fluorescence upon application of 100 μM HA (Fig. 1f-i) and
101 an EC50 of 380 nM when expressed in HEK293T cells (Fig. 1j).

102   We then characterized the kinetic properties and wavelength spectrum of the HA sensors. Using
103 a local perfusion system and high-speed line-scanning, both HA1h and HA1m had a rapid increase
104 in fluorescence in response to a saturating concentration of HA, with an on-rate (time constant) of
105 0.6 s and 0.3 s, respectively (Fig. 2a-c). The off-rate of HA1h and HA1m was measured by rapidly
106 applying H_4R and H_1R antagonists, respectively, yielding an off-rate (time constant) of 2.3 s (HA1m)
107 and 1.4 s (HA1m) (Fig. 2a-c). Both HA1h and HA1m had a similar spectrum as EGFP, with an
108 excitation peak at ~505 nm and an emission peak at ~520 nm under one-photon illumination, and
109 an excitation peak at ~920 nm under two-photon illumination (Supplementary Fig. 3a).

110   Next, we tested whether our HA sensors can trigger downstream signaling pathways, including
111 G protein–dependent and/or β-arrestin–dependent pathways. Because human H_4R is a Gi-coupled
112 G protein–coupled receptor (GPCR), we used a chimeric $G\alpha_{q-i}$ protein, which switches the
113 downstream response from Gi to Gq signaling[21,22]. Using intracellular Ca^{2+} imaging, we found that
114 the hH_4Rs and water bear H_1Rs signaled robustly, whereas both the HA1h and HA1m sensors
115 produced virtually no response (Fig. 2d). Similar results were obtained when we measured signaling
116 via the β-arrestin pathway using the Tango assay (Fig. 2e). Furthermore, consistent with our Tango
117 assay results, we found that exposing HA1h- and HA1m-expressing cultured neurons to a saturating
118 concentration of HA for 3 h led to virtually no internalization of either sensor (Supplementary Fig.
119 4a,b). Taken together, these results suggest that our HA sensors can be used to measure extracellular
120 HA without inadvertently activating downstream signaling pathways.

121   To measure the performance of our HA sensors in a more physiologically relevant context, we
122 expressed HA1h, HA1m, or HA1mut in cultured rat cortical neurons using an adeno-associated
123 virus (AAV). We found that HA1h and HA1m localize throughout the neuronal plasma membrane
124 (Fig. 2f). Moreover, bath application of a saturating concentration of HA caused a robust increase
125 in both HA1h and HA1m fluorescence (with peak $\Delta F/F_0$ values of approximately 180% and 320%,
126 respectively), with no measurable effect on HA1mut (Fig. 2g,h). In addition, similar to our results
127 obtained with HEK293T cells, we found that neurons expressing either HA1h or HA1m had a dose-
128 dependent increase in fluorescence, with EC50 values of 19 nM and 400 nM, respectively (Fig. 2i).
129 To confirm the specificity of our sensors for HA, we tested the effects of an HA precursor, several
130 HA metabolites, and several monoamines and neurotransmitters, finding no measurable response to
131 any of these compounds (Fig. 2j). Notably, the HA-induced response in HA1h and HA1m was fully
132 blocked by the H_4R antagonist JNJ-7777120 and the H_1R antagonist clemastine, respectively, while

133 all other HA receptor antagonists had no effect (Fig. 2j). Consistently, the HA-induced response in

134 HA1h and HA1m was specifically blocked by the H_4R antagonist and the H_1R antagonist in cultured

135 HEK293T cell systems (Supplementary Fig. 3b), respectively. Furthermore, radioligand binding

136 assay was performed to test whether HA sensors specifically are bound by HA. We found HA and

137 the H_4R agonist N^α-methylhistamine to specifically bind to HA1h sensor, while HA precursor and

138 HA metabolites, and several monoamines and neurotransmitters had no measurable binding

139 (Supplementary Fig. 5b). Together, these results indicate that both HA1h and HA1m retain the

140 pharmacological profile and ligand specificity of their corresponding parent receptors.

141

GRAB$_{HA}$ sensors can be used to image HA release in acute mouse brain slices

143 Next, we examined whether our HA sensors can be used to detect the release of endogenous HA.

144 We therefore injected an AAV expressing HA1m under the control of the human synapsin (hSyn)

145 promoter into the mouse prefrontal cortex (PFC) and prepared acute brain slices 2-3 weeks later

146 (Fig. 3a,b). We found that applying electrical stimuli at 20 Hz elicited a pulse number–dependent

147 increase in HA1m fluorescence that was blocked by treating the slices with the H_1R antagonist

148 clemastine (Fig. 3c,d). We also measured the kinetics of the response to 10, 20, 50, and 100 pulses

149 delivered at 20 Hz and obtained rise time constants (τ_{on}) and decay time constants (τ_{off}) of 1.4-5.2 s

150 and 10-13 s, respectively (Fig. 3e). Interestingly, we also found that the HA1m signal increased at

151 the site of stimulation and then propagated outward (Fig. 3f). We measured the change in

152 fluorescence at various distances from stimulation site at various time points and obtained an

153 apparent diffusion coefficient of approximately 1.9×10^3 $\mu m^2/s$ (Fig. 3g-j). Thus, our HA1m sensor

154 can detect the release of endogenous HA with high spatiotemporal resolution.

155

GRAB$_{HA}$ sensors can be used to measure HA release *in vivo*

157 A wealth of pharmacological and genetic data has shown that HA plays an essential role in regulating

158 the sleep-wake cycle[23]. Thus, based on these findings we examined whether our HA sensors could

159 be used to measure histaminergic activity during the physiological sleep-wake cycle, focusing on

160 the transitions between sleep-wake states. In the mammalian brain, the preoptic area (POA)

161 regulates sleep and receives extensive projections from histaminergic neurons[24,25]. We expressed

162 the HA1m sensor in the POA and then performed simultaneous fiber photometry,

163 electroencephalography (EEG), and electromyography (EMG) recordings in freely behaving mice

164 (Fig. 4a). We found that the signal produced by the HA1m sensor in the POA was relatively high

165 when the mouse was awake compared to the signal measured during both rapid eye movement

166 (REM) and non-REM (NREM) sleep (Fig. 4b,c), supporting previously reported data obtained using

167 microdialysis[26]. As a control, we also expressed the HA1m sensor in the POA of histidine

168 decarboxylase knockout (HDC KO) mice and found no significant change in HA1m fluorescence

169 at any stage during the sleep-wake cycle (Fig. 4d). Because our HA sensors have rapid kinetics, we

170 then calculated the change in HA1m signal at the transitions between various sleep states and found

171 that the signal increased during the REM→wake and NREM→wake transitions, but decreased

172 during the wake→NREM and NREM→REM transitions (Fig. 4f).

173 We recorded HA release in the POA using our medium-affinity HA1m sensor, as the POA

174 receives a relatively dense number of histaminergic projections. Next, we examined whether we

175 could measure HA release in the prefrontal cortex (PFC), a brain region that receives a more

176 moderate density of histaminergic projections and plays a critical role in regulating executive

177   functions such as attention and decision, functions that are based on wakefulness. To account for
178   the lower density of histaminergic projections, we expressed the high-affinity HA1h sensor in the
179   PFC and performed simultaneous fiber photometry, EEG, and EMG recordings in freely behaving
180   mice (Fig. 5a). Similar to our results obtained using the HA1m sensor expressed in the POA, we
181   found that the HA1h signal in the PFC was higher when the animal was awake compared to during
182   both REM and NREM sleep (Fig. 5b,c), again consistent with previously reported microdialysis
183   data [27]. As expected, consistent with our *in vitro* results, an i.p. injection of the H_4R antagonist JNJ-
184   7777120 virtually eliminated fluorescence of the HA1h sensor expressed in the PCF, even when the
185   mouse was awake (Fig. 5d,e). Furthermore, no significant change in fluorescence was measured in
186   the PFC of mice expressing the mutant HA1mut sensor at any time during the sleep-wake cycle (Fig.
187   5f,g). Finally, no significant attenuation in HA1h sensor signals over one day recording under low
188   excitation light intensity and sample rate (Supplementary Fig. 7a-c).
189   HA is believed to play an important role in both the initiation and maintenance of wakefulness[23].
190   Thus, the histamine H3 receptor H_3R is a novel promising target for improving vigilance, and the
191   H_3R antagonist ciproxifan may have potential therapeutic benefits in the context of vigilance
192   deficiency[28]. In addition, the stimulant caffeine is widely used to maintain wakefulness. We
193   therefore used our HA sensors to determine whether ciproxifan and/or caffeine mediate their effects
194   on wakefulness by increasing HA release (Fig. 5h). As expected, we found that both ciproxifan and
195   caffeine prolonged wakefulness in mice (Fig. 5i,j). Interestingly, however, we found that
196   ciproxifan—but not caffeine—increased the fluorescence signal of HA1h expressed in the PFC (Fig.
197   5i-k, Supplementary Fig. 6a-c). we further confirm that ciproxifan also increased the fluorescence
198   signal of HA1m expressed in POA in wild type mice, but not HDC KO mice (Supplementary Fig.
199   6d-f). These results indicate that although both ciproxifan and caffeine promote wakefulness, they
200   do so via distinct mechanisms, with ciproxifan, but not caffeine, increasing HA release in the PFC.
201

The kinetics of HA release differ in different brain regions

203   Histaminergic neurons send their projections to numerous target regions throughout the brain[24]. We
204   therefore asked whether the temporal pattern of HA release is universal throughout the brain or
205   differs among various brain regions. As a first step toward addressing this question, we expressed
206   the HA1h sensor in both the PFC and POA and then simultaneously recorded the fluorescence
207   signals in these two nuclei (Fig. 6a). We found that the magnitude of the HA1h signal measured at
208   each state in the sleep-wake cycle was similar between the PFC and POA (Fig. 6b,c). We also found
209   a close temporal cross-correlation in the time-shift data (Fig. 6d), indicating that the signal change
210   in the POA preceded the signal change in the PFC. We then aligned and normalized the signals
211   measured during the wake-sleep state transitions and found that the signals measured in the POA
212   were faster than the corresponding signals measured in the PFC during both the REM→wake
213   transition, the NREM→wake transition, and the wake→NREM transition (Fig. 6e). We also
214   quantified the kinetics of the responses by calculating the t_{50} value of the signal rise or fall at each
215   transition. We found that that the t_{50} values measured in the POA were significantly lower than the
216   corresponding values measured in the PFC during the REM→wake, NREM→wake, and
217   wake→NREM transitions, but were similar during the NREM→REM transition (Fig. 6f), indicating
218   a clear difference in HA release kinetics between the POA and PFC (summarized schematically in
219   Fig. 6g). These results raise at least two possibilities: first, histaminergic projections in the POA and
220   PFC may arise from different subpopulations of histaminergic neurons; alternatively, HA release

221 may be modulated by other neurotransmitters and modulators acting locally at the site of
222 histaminergic innervation (Supplementary Fig. 8).
223

224 **Discussion**
225 Here, we report the development and characterization of two genetically encoded GPCR activation–
226 based fluorescent sensors for measuring changes in extracellular HA in real time. With their high
227 sensitivity, high selectivity, and rapid kinetics, GRAB$_{HA}$ sensors can reliably detect endogenous HA
228 release both *in vitro* and in freely behaving animals under physiological conditions.
229 Our GRAB$_{HA}$ sensors offer several clear advantages over existing methods for measuring HA.
230 First, GRAB$_{HA}$ sensors have high sensitivity and a relatively high signal-to-noise ratio in response
231 to HA. Specifically, the HA1h and HA1m sensors produce a peak fluorescence response of ~300%
232 and 500%, respectively, with an apparent affinity of ~20 nM and 400 nM, respectively. In contrast,
233 GPCR-based FRET[12] and BRET[13] probes for detecting HA have a low peak response of ~160% (or
234 only 25% under optimal conditions) and are limited to use in *in vitro* applications. Second, our
235 GRAB$_{HA}$ sensors have rapid kinetics, with rise and decays times of 0.3-0.6 s and 1.4-2.3 s,
236 respectively. Although this response time of GRAB$_{HA}$ sensors is slightly longer than fast-scan cyclic
237 voltammetry, it is sufficient to report physiologically relevant changes in HA levels and is similar
238 to the response times reported for wild-type GPCRs[29] and other GRAB sensors[16,20,30]. In addition,
239 our GRAB$_{HA}$ sensors have high spatial resolution and are photostable, allowing for stable recordings
240 over prolonged experiments. Finally, our sensors have high specificity for HA, as they can reliably
241 detect changes in extracellular HA in wild-type mice, but produce no signal in knockout mice
242 lacking the enzyme histidine decarboxylase (HDC). Building on these key advantages over other
243 tools, we used our GRAB$_{HA}$ sensors to measure the release and apparent diffusion rate of HA in
244 acute brain slices by combining the sensor with two-photon imaging. In addition, we combined our
245 sensors with fiber photometry recording to monitor real-time changes in histaminergic activity in
246 the mouse brain during the sleep-wake cycle.
247 Our GRAB$_{HA}$ sensors have the same high specificity for HA and pharmacological profile of
248 their corresponding parent receptors. Using cultured neurons, we found that both the human and
249 tardigrade receptor-derived HA sensors respond to HA, but do not respond to an HA precursor, HA
250 metabolites, or any other neurotransmitters tested. Similarly, each sensor's signal was blocked by
251 the corresponding receptor antagonists, but was unaffected by other HA receptor antagonists,
252 indicating that the complementary pharmacological profile of these two HA sensors can be exploited
253 in order to study how HA release is regulated by various compounds that target histaminergic
254 signaling. For example, the H$_3$R receptor is a promising new target for improving vigilance, and an
255 H$_3$R antagonist has been shown to increase HA turnover by blocking the negative feedback
256 regulation of HA release (see Fig. 5h)[31,32]. Consistent with these previous studies, we found that the
257 GRAB$_{HA}$ response was larger in wild-type mice that received an H$_3$R antagonist, but was not
258 affected in HDC-deficient mice (see Supplementary Fig. 6d-f), indicating that our HA sensors can
259 be used to monitor the effects of H$_3$R antagonists on histaminergic signaling.
260 Using our GRAB$_{HA}$ sensor, we also found that specific brain regions have distinct patterns of
261 HA release kinetics. This finding suggests that the projections of histaminergic neurons are
262 heterogenous; however, an alternative possibility is that HA release may be modulated to some
263 extent by local or regional neurotransmitters, modulators, and/or pathways (Supplementary Fig. 8).
264 In the brain, histaminergic projections: *i*) originate from a single source, namely the

265   tuberomammillary nucleus (TMN) in the posterior hypothalamus; *ii*) innervate nearly all regions of
266   the brain; and *iii*) regulate a wide range of behaviors and processes. Histaminergic TMN neurons
267   are organized into five clusters, E1 through E5 [33,34]; however, retrograde tracers injected into various
268   brain regions labeled the entire TMN, without any clear topographical pattern[33,35]. By combining
269   cell type–specific sparse labeling with fluorescence micro-optical sectioning tomography, whole-
270   brain histaminergic axonal projection mapping revealed that histaminergic neurons indeed send
271   heterogeneous projections to their downstream target regions[36]. With respect to the second
272   possibility, several studies have shown that neurotransmitter release can be modulated at the level
273   of the axon terminal. For example, dopamine release in the striatum is regulated at the axon terminal
274   by acetylcholine[37,38]. Thus, HA release may also be modulated by the local environment, giving rise
275   to our observation of heterogeneous release dynamics among target regions. Future studies
276   combining our GRAB$_{HA}$ sensors with other tools and strategies may shed new light on the
277   mechanism underlying HA release and its regulation at the local and/or regional level.
278   In addition to regulating the sleep-wake cycle, HA plays a role in a number of physiological
279   and pathological processes in the central nervous system, including feeding, motor control,
280   cognition, narcolepsy, epilepsy, migraine, and Tourette's syndrome[39,40]. Interestingly, HA also
281   serves as the primary neurotransmitter for visual input in *Drosophila* photoreceptors[41,42]. Moreover,
282   histamine plays a major role in allergic responses, including anaphylaxis[1]. Thus, this novel set of
283   HA sensors suitable for both *in vitro* and *in vivo* applications can be used to measure HA release in
284   a variety of settings and models, providing valuable new insights into the role of histaminergic
285   signaling in both health and disease.

286 **Methods**

287 **Animals**

288 All experimental procedures involving animals were performed in accordance with the guidelines

289 established by the Animal Care and Use Committee at Peking University. Wild-type C57BL/6j mice

290 were obtained from the Beijing Vital River Laboratory and used to prepare the acute brain slices

291 and for some *in vivo* mouse experiments. Histidine decarboxylase knockout (HDC KO) mice (on a

292 BALB/c background) were kindly provided by Dr. Xiangdong Yang at Fudan University; HDC KO

293 and control littermates were used for *in vivo* recordings. Newborn wild-type Sprague-Dawley rat

294 pups (P0) were obtained from the Beijing Vital River Laboratory and used to prepare primary

295 cortical neuron cultures. All animals were housed at 18–23°C in 40–60% humidity under a 12/12-h

296 light/dark cycle, with food and water available *ad libitum*.

297

298 **Molecular biology**

299 The clones used in this study were generated using the Gibson assembly method. DNA fragments

300 were amplified by PCR using primers (TSINGKE Biological Technology) with 25–30-bp overlap

301 and then assembled using T5 exonuclease (New England Biolabs), Phusion DNA polymerase

302 (Thermo Fisher Scientific), and Taq ligase (iCloning). All plasmid sequences were verified using

303 Sanger sequencing (TSINGKE Biological Technology). To characterize the sensors in HEK293T

304 cells, all cDNAs encoding the candidate $GRAB_{HA}$ sensors were cloned into the pDisplay vector with

305 an upstream IgK leader sequence and a downstream IRES-mCherry-CAAX cassette to label the cell

306 membrane and calibrate the sensor's fluorescence intensity. To characterize the sensors in cultured

307 neurons, sequences encoding HA1h, HA1m, and HA1mut were cloned into the pAAV vector

308 containing the human synapsin (hSyn) promoter. To measure downstream signaling using the Tango

309 assay, genes encoding wild-type H_1R and H_4R, as well as the HA1h and HA1m sensors, were cloned

310 into the pTango vector. To characterize the sensors' wavelength spectra, sequences encoding HA1h

311 and HA1m were cloned into the pPacific vector containing a 3′ terminal repeat, IRES, puromycin

312 gene, and a 5′ terminal repeat. Two mutations (S103P and S509G) were introduced into the pCS7-

313 PiggyBAC vector (ViewSolid Biotech) to generate a hyperactive piggyBac transposase, which was

314 used to generate stable cell lines expressing HA1h or HA1m.

315

316 **Recombinant adeno-associated virus (AAV)**

317 AAV2/9-hSyn-HA1h (2.64×10^{13} GC/ml, WZ Biosciences), AAV2/9-hSyn-HA1m (3.92×10^{13}

318 GC/ml, WZ Biosciences), and AAV2/9-hSyn-HA1mut (9.03×10^{13} GC/ml, WZ Biosciences) were

319 used to infect cultured neurons or were injected into specific mouse brain regions.

320

321 **Cell culture**

322 HEK293T cells were purchased from ATCC and verified based on their morphology observed by

323 microscopy and an analysis of their growth curve; the cells were cultured at 37°C in humidified air

324 containing 5% CO_2 in DMEM (Biological Industries) supplemented with 10% (v/v) FBS (Gibco),

325 penicillin (100 U/ml), and streptomycin (0.1 mg/ml) (Biological Industries). For expressing the

326 $GRAB_{HA}$ sensors, HEK293T cells were plated on 96-well plates or 12-mm glass coverslips in 24-

327 well plates and grown to 60-70% confluence, and then transfected using polyethylenimine (PEI)

328 with 300 ng DNA per well (for 96-well plates) or 1 µg DNA per well (for 24-well plates) at a

329 DNA:PEI ratio of 1:3. The culture medium was replaced with fresh medium 6-8 h after transfection,

330 and fluorescence imaging was performed 24–48 h after transfection.

331 Rat cortical neurons were prepared from P0 Sprague-Dawley rat pups. In brief, the cortex was

332 dissected, and the neurons were dissociated in 0.25% trypsin–EDTA (Gibco), plated on 12-mm glass

333 coverslips coated with poly-D-lysine (Sigma-Aldrich), and cultured in neurobasal medium (Gibco)

334 containing 2% B-27 supplement (Gibco), 1% GlutaMAX (Gibco), and 1% penicillin-streptomycin

335 (Gibco) at 37°C in humidified air containing 5% CO_2. For viral infection, cultured neurons were

336 infected with AAV2/9-hSyn-HA1h, AAV2/9-hSyn-HA1m, or AAV2/9-hSyn-HA1mut at 3–5 days

337 *in vitro* (DIV3–DIV5), and fluorescence imaging was performed at DIV10–DIV14.

338

339 **Fluorescence imaging of cultured cells**

340 Cultured cells were imaged using the Opera Phenix high-content screening system (PerkinElmer)

341 and an inverted Ti-E A1 confocal microscope equipped with a 20x 0.4-numerical aperture (NA)

342 objective, a 40x 0.6-NA objective, a 40x 1.15-NA water-immersion objective, a 488-nm laser, and

343 a 561-nm laser. A 525/50 nm emission filter and a 600/30 nm emission filter were used to collect

344 the GFP and RFP signals, respectively.

345 During fluorescence imaging, cells expressing the $GRAB_{HA}$ sensors were first bathed in

346 Tyrode's solution and then imaged before and after addition of the indicated drugs at various

347 concentrations. The change in fluorescence intensity of the $GRAB_{HA}$ sensors was calculated using

348 the change in the GFP/RFP ratio and is expressed as $\Delta F/F_0$.

349 To measure the response kinetics of $GRAB_{HA}$ sensors in the rapid perfusion experiments using

350 the line-scanning mode, the tip of a glass pipette containing 100 μM HA was placed near the sensor-

351 expressing HEK293T cells. HA was puffed onto the cells from the pipette to measure the on-rate.

352 To measure the off-rate, 1 mM of the appropriate antagonist (JNJ-7777120 to block HA1h,

353 clemastine to block HA1m) was applied using a glass pipette to sensor-expressing cells bathed in

354 HA (1 μM HA for cells expressing HA1h, 10 μM HA for cells expressing HA1m).

355

356 **Spectra measurements**

357 For the HA1h sensor, HEK293T cells stably expressing HA1h under the control of CAG promoter

358 were plated in a 384-well plate in the absence or presence of 100 μM HA. Control cells used for

359 background subtraction were transfected with an empty vector. Using a Safire[2] multi-mode plate

360 reader (Tecan), excitation spectra were measured from 300 to 520 nm at 5-nm increments and a

361 bandwidth of 20 nm, while the emission spectrum was set to 560 nm with a 20-nm bandwidth.

362 Emission spectra were measured from 500 to 700 nm at 5-nm increments and a bandwidth of 20 nm,

363 while the excitation spectrum was set to 455 nm with a bandwidth of 20 nm. For the HA1m sensor,

364 the plasmid expressing HA1m or an empty vector was transfected into HEK293T cells in 6-well

365 plates; 24–36 h after transfection, the cells were harvested using trypsin, washed with PBS,

366 resuspended in Tyrode's solution in the absence or presence of 100 μM HA, and plated into a 384-

367 well plate, followed by the spectra measurements described above.

368

369 **G_{qi} calcium imaging assay**

370 Plasmids expressing the $GRAB_{HA}$ sensors, H_1R-EGFP, or H_4R-EGFP were co-transfected with a

371 construct expressing jRGECO1a-P2A-G_{q-i1} into HEK293T cells plated on 12-mm coverslips; 24–

372 48 h after transfection, the cells were imaged using a Ti-E A1 confocal microscope (Nikon) as

373 described above. The indicated concentrations of HA were then applied by bath application and

374   removed using a custom-made perfusion system.

375

376   **Tango assay**

377   Plasmids expressing wild-type H_1R, wild-type H_4R, HA1h, or HA1m were transfected into HTLA

378   cells in 6-well plates; 24 h after transfection, the cells were harvested using trypsin and plated in 96-

379   well plates. HA was then applied at a final concentration ranging from 1 nM to 1 mM, and the cells

380   were cultured for an additional 12 h to allow for luciferase expression. Bright-Glo (Luciferase Assay

381   System, Promega) was then added to a final concentration of 5 μM, and luminescence was measured

382   using a VICTOR X5 multilabel plate reader (PerkinElmer).

383

384   **[^{3}H]histamine competition binding assay**

385   Plasmids expressing wild-type H_4R or HA1h were transfected into HEK293T cells in 10 cm dishes;

386   48 h after transfection, the cells were collected, centrifuged at 2000g for 10 min at 4°C, resuspended

387   in 50 mM Tris-HCl binding buffer (pH7.4), and sonicated for 10 sec using a Branson sonifier 250

388   (Boom bv., Meppel, The Netherlands). The cell homogenates were incubated with ~8.5 nM [^{3}H]-

389   histamine in the absence of presence of 30 μM unlabeled compounds in a total volume of 100 μl/well

390   at 25°C on a shaker (600 rpm). After 2 h, the incubations were terminated by rapid filtration through

391   0.5% (v/v) polyethylenimine pre-soaked GF/C filterplates using a 96-well Filtermate harvester

392   (PerkinElmer), followed by four rapid washes with ice-cold binding buffer. The GF/C filterplates

393   were dried at 52°C and 25 μl Microscint-O was added to each well to quantify radioactivity using a

394   Microbeta Wallac Trilux scintillation counter (PerkinElmer). Saturation binding of [^{3}H]histamine

395   was measured with increasing concentrations of [^{3}H]histamine in the absence or presence of 50

396   microM JNJ7777120 to detect total and nonspecific binding respectively. The binding affinity (K_d)

397   values were determined using nonlinear fitting (One site – total and nonspecific binding) in

398   GraphPad Prism 9.4.0.

399

400   **Two-photon fluorescence imaging of mouse acute brain slices**

401   For AAV injection, adult wild-type C57BL/6N mice were firstly anesthetized by an i.p. injection of

402   Avertin (500 mg/kg, Sigma-Aldrich), and then fixed in a stereotaxic frame (RWD Life Science) for

403   injection of the AAV expressing hSyn-HA1m (300 nl per site) using a micro-syringe pump

404   (Nanoliter 2000 Injector, World Precision Instruments). The AAV was injected into the PFC of the

405   left hemisphere of C57BL/6N mice using the following coordinates: AP: +1.9 mm relative to

406   Bregma, ML: -0.3 mm, and DV: -1.8 mm below the dura.

407   For slice preparation, 2-3 weeks after virus injection, mice were deeply anesthetized again with

408   an i.p. injection of Avertin, and then transcardial perfusion was rapidly performed using cold

409   oxygenated slicing buffer containing (in mM): 110 Choline-Cl, 25 $NaHCO_3$, 25 Glucose, 7 $MgCl_2$,

410   2.5 KCl, 1.3 Na ascorbate, 1 NaH_2PO_4, 0.5 $CaCl_2$, and 0.6 Na pyruvate. The isolated brains were

411   subsequently immersed into the oxygenated slicing buffer, and the cerebellum was trimmed using a

412   razor blade. The caudal sides were then glued on the cutting stage of a VT1200 vibratome (Leica)

413   and sectioned into 300-μm thick coronal slices. Brain slices containing the PFC region were

414   incubated at 34°C for ~40 min in the oxygen-saturated Ringer's buffer containing (in mM): 125

415   NaCl, 25 $NaHCO_3$, 25 Glucose, 2.5 KCl, 2 $CaCl_2$, 1.3 $MgCl_2$, 1.3 Na ascorbate, 1 NaH_2PO_4, and

416   0.6 Na pyruvate.

417   For two-photon imaging, the HA1m-expressing slices were transferred into a perfusion chamber

418   in an Ultima Investigator 2P microscope (Bruker) equipped with a 25× /1.05-NA water-immersion
419   objective and a mode-locked Mai Tai Ti: Sapphire laser (Spectra-Physics). The laser wavelength
420   was tuned to 920 nm for measuring the fluorescence of HA1m using a 495-540 nm filter. A
421   homemade bipolar electrode (cat. #WE30031.0A3, MicroProbes) was placed onto the slice surface
422   near the PFC under fluorescence guidance. Fluorescence was then recorded at video frame rates of
423   0.3259 s/frame, with a resolution of 256×256 pixels. The stimulation voltage was set at 4-6 V with
424   the duration of each stimulation at 1 ms. Stimulation and imaging were synchronized through a
425   custom-written program running on an Arduino board.

426

427   Surgery for virus injection, placement of EEG and EMG electrodes, and fiber implantation
428   Adult mice were anesthetized with 1.5% isoflurane, and 2% lidocaine hydrochloride was injected
429   subcutaneously under the scalp; the mouse was then placed on a stereotaxic frame (RWD Life
430   Science). The skull was exposed, and small craniotomy holes were prepared for virus injection, into
431   which a total of approximately 300 nl AAV9-hSyn-HA1h, AAV9-hSyn-HA1m, or AAV9-hSyn-
432   HA1mut virus was microinjected into the PFC (AP: +1.9 mm relative to Bregma, ML: -0.3 mm,
433   DV: 1.9 mm below the dura) and/or POA (AP: 0 mm relative to Bregma, ML: -0.6 mm, DV: 4.9
434   mm below the dura) via a fine glass pipette and micro-syringe pump (Nanoliter 2010 injector, World
435   Precision Instruments).
436   For recording the fluorescence signals, a 200-μm optical fiber cannula (Fiber core: 200 μm;
437   numerical aperture: 0.37; Inper, Zhejiang, China) was implanted 0.1 mm above the virus injection
438   sites.
439   To record the animal's sleep-wake state, EEG electrodes were implanted into the craniotomy
440   holes over the frontal cortex and visual cortex, and EMG wires were placed bilaterally into the
441   trapezius muscles. The electrodes were attached to a microconnector and fixed to the skull using
442   dental cement.

443

444   Fiber photometry recording and analysis
445   A fiber photometry system (Thinker Tech, Nanjing, China) was used to record the fluorescence
446   signals in freely moving mice. Blue (473-nm) LED light (Cree LED) was bandpass filtered (470/25
447   nm, model 65-144, Edmund Optics), reflected by a dichroic mirror (model 67-069, Edmund Optics),
448   and then focused using a 20x objective lens (Olympus). An optical fiber guided the light between
449   the commutator and the implanted optical fiber cannula. The excitation light power at the tip of the
450   optical fiber was adjusted 20-30 μW and delivered at 100 Hz with 5 ms pulse duration when the
451   recording lasted <24 h; the light power was adjusted to a lower level (10-20 μW) and was delivered
452   at 10 Hz when the recording lasted >24 h in order to minimize photobleaching. The green
453   fluorescence was bandpass filtered (525/25 nm, model 86-354, Edmund Optics) and collected using
454   a photomultiplier tube (model H10721-210, Hamamatsu). An amplifier (model C7319, Hamamatsu)
455   was used to convert the current output from the photomultiplier tube to a voltage signal and was
456   passed through a low-pass filter. The analog voltage signals were then digitized using an acquisition
457   card (National Instruments). To minimize autofluorescence of the optical fiber, the recording fiber
458   was photobleached using a high-power LED before recording. Background autofluorescence was
459   subtracted from the recorded signals in the subsequent analysis.
460   The photometry data were analyzed using a custom program written in MATLAB. To calculate
461    $\Delta F/F_0$, baseline values were measured during REM sleep with no apparent fluctuations. To compare

462   the change in fluorescence between animals, the *z*-score–transformed $\Delta F/F_0$ was further normalized

463   using the standard deviation of the baseline signals.

464

465   **Polysomnographic recording and analysis**

466   We used the EEG and EMG recordings to determine the animal's sleep-wake state. The EEG and

467   EMG electrode microconnectors were connected via a flexible cable and attached to an electric slip

468   ring to allow the mice to move freely. The cortical EEG and neck EMG signals were amplified

469   (NL104A, Digitimer), filtered (NL125/6, Digitimer), digitized using a Power1401 digitizer

470   (Cambridge Electronic Design Ltd.), and recorded using Spike2 software (Cambridge Electronic

471   Design Ltd.) at a sampling rate of 1000 Hz. The polysomnographic signals were filtered (EEG: 0.5-

472   100 Hz, EMG: 30-500 Hz) and semi-automatically scored off-line in 4-s epochs of wakefulness,

473   REM sleep, and NREM sleep using AccuSleep (https://github.com/zekebarger/AccuSleep) [43]; the

474   defined sleep-wake stages were examined visually and corrected if necessary. Wakefulness was

475   defined as desynchronized low-amplitude EEG activity and high-amplitude EMG activity with

476   phasic bursts. NREM sleep was defined as synchronized EEG with high-amplitude delta rhythm

477   (0.5-4 Hz) and low EMG activity. REM sleep was defined as a pronounced theta rhythm (6-10 Hz)

478   and low EMG activity. EEG spectral analysis was estimated using a short-time fast Fourier

479   transform (FFT).

480

481   **Quantification and statistical analysis**

482   The animals and cells in the experiments were randomly assigned to different groups at sample sizes

483   that were determined based on previous studies[44]. Imaging data from cultured HEK293T cells,

484   cultured rat cortical neurons, and acute mouse brain slices were processed using ImageJ software

485   (NIH) and analyzed using custom MATLAB code. Exponential-function fitting was used to correct

486   for slight photobleaching. Background levels measured outside the region of interest in the

487   pseudocolor images were subtracted using ImageJ.

488   Origin 2020 (OriginLab) and Prism 8 & 9 (GraphPad) were used to perform the statistical

489   analyses. Except where indicated otherwise, all summary data are presented as the mean ± sem. The

490   paired or unpaired Student's *t*-test was used to compare two groups, and a one-way analysis of

491   variance (ANOVA) was used to compare more than two groups. All statistical tests were two-tailed,

492   and differences were considered statistically significant at $P < 0.05$.

493

494   **Data and code availability**

495   Plasmids expressing the sensors used in this study were deposited at Addgene (Addgene ID, HA1h,

496   190473. HA1m, 190474. HA1mut 190475). The data and custom-written ImageJ macro, Arduino,

497   and MATLAB programs are available upon request to the corresponding author.

498

499   **Acknowledgments**

506 and the National Center for Protein Sciences at Peking University in Beijing, China, for support and
507 assistance with the Opera Phenix high-content screening system and imaging platform. We thank
508 Xiangdong Yang at Fudan University kindly provided HDC KO mice. Some graphics were
509 generated using BioRender.com.
510

Author contributions

512 Y.L. conceived and supervised the project. M.L. performed the experiments related to developing,
513 optimizing and characterizing the sensor in cultured HEK293T cells and neurons. Y.Y. characterized
514 HA sensors in HEK293T cells and neurons. X.M and H.F.V performed the binding studies. T.Q. and
515 M.L. performed the experiments in brain slices. H.D., Y.L., and C.L. performed the *in vivo* recording
516 in behaving mice. G.L. and H.W. performed the characterization of the wavelength spectra of HA
517 sensors in HEK293T cells. All authors contributed to data interpretation and analysis. Y.L., H.D.,
518 and Y.Y. wrote the manuscript with input from all other authors.
519

Competing interests

521 Y.L. have filed patent applications, the value of which might be affected by this publication. The
522 remaining authors declare no competing interests.

Reference

1   White, M. The role of histamine in allergic diseases. *Journal of Allergy and Clinical Immunology* **86**, 599-605, doi:10.1016/s0091-6749(05)80223-4 (1990).

2   Prinz, C., Zanner, R. & Gratzl, M. Physiology of gastric enterochromaffin-like cells. *Annu Rev Physiol* **65**, 371-382, doi:10.1146/annurev.physiol.65.092101.142205 (2003).

3   Faingold, C. L. in *Histamine II and Anti-Histaminics: Chemistry, Metabolism and Physiological and Pharmacological Actions*   (ed Mauricio Rocha e Silva)   561-573 (Springer Berlin Heidelberg, 1978).

4   Watanabe, T. *et al.* Evidence for the presence of a histaminergic neuron system in the rat brain: An immunohistochemical analysis. *Neuroscience Letters* **39**, 249-254, doi:10.1016/0304-3940(83)90308-7 (1983).

5   Haas, H. & Panula, P. The role of histamine and the tuberomamillary nucleus in the nervous system. *Nat Rev Neurosci* **4**, 121-130, doi:10.1038/nrn1034 (2003).

6   Yoshitake, T. *et al.* Determination of histamine in microdialysis samples from rat brain by microbore column liquid chromatography following intramolecular excimer-forming derivatization with pyrene-labeling reagent. *J Neurosci Methods* **127**, 11-17, doi:10.1016/s0165-0270(03)00097-9 (2003).

7   Puthongkham, P., Lee, S. T. & Venton, B. J. Mechanism of Histamine Oxidation and Electropolymerization at Carbon Electrodes. *Analytical Chemistry* **91**, 8366-8373, doi:10.1021/acs.analchem.9b01178 (2019).

8   Cash, K. J. & Clark, H. A. Phosphorescent nanosensors for in vivo tracking of histamine levels. *Anal Chem* **85**, 6312-6318, doi:10.1021/ac400575u (2013).

9   Barnea, G. *et al.* The genetic design of signaling cascades to record receptor activation. *Proc Natl Acad Sci U S A* **105**, 64-69, doi:10.1073/pnas.0710487105 (2008).

10   Kroeze, W. K. *et al.* PRESTO-Tango as an open-source resource for interrogation of the druggable human GPCRome. *Nat Struct Mol Biol* **22**, 362-369, doi:10.1038/nsmb.3014 (2015).

11   Jagadish, S., Barnea, G., Clandinin, T. R. & Axel, R. Identifying functional connections of the inner photoreceptors in Drosophila using Tango-Trace. *Neuron* **83**, 630-644, doi:10.1016/j.neuron.2014.06.025 (2014).

12   Liu, Y. *et al.* Visualization of the activation of the histamine H3 receptor (H3R) using novel fluorescence resonance energy transfer biosensors and their potential application to the study of H3R pharmacology. *FEBS J* **285**, 2319-2336, doi:10.1111/febs.14484 (2018).

13   Schihada, H. *et al.* Development of a Conformational Histamine H3 Receptor Biosensor for the Synchronous Screening of Agonists and Inverse Agonists. *ACS Sens* **5**, 1734-1742, doi:10.1021/acssensors.0c00397 (2020).

14   Erdogmus, S. *et al.* Helix 8 is the essential structural motif of mechanosensitive GPCRs. *Nat Commun* **10**, 5784, doi:10.1038/s41467-019-13722-0 (2019).

15   Jing, M. *et al.* A genetically encoded fluorescent acetylcholine indicator for in vitro and in vivo studies. *Nat Biotechnol* **36**, 726-737, doi:10.1038/nbt.4184 (2018).

16   Sun, F. *et al.* A Genetically Encoded Fluorescent Sensor Enables Rapid and Specific Detection of Dopamine in Flies, Fish, and Mice. *Cell* **174**, 481-496 e419, doi:10.1016/j.cell.2018.06.042 (2018).

17   Dong, A. *et al.* A fluorescent sensor for spatiotemporally resolved imaging of

567 endocannabinoid dynamics in vivo. *Nat Biotechnol* **40**, 787-798, doi:10.1038/s41587-
568 021-01074-4 (2022).

569 18 Patriarchi, T. *et al.* Ultrafast neuronal imaging of dopamine dynamics with designed
570   genetically encoded sensors. *Science* **360**, doi:10.1126/science.aat4422 (2018).

571 19 Wu, Z., Lin, D. & Li, Y. Pushing the frontiers: tools for monitoring neurotransmitters and
572   neuromodulators. *Nat Rev Neurosci*, doi:10.1038/s41583-022-00577-6 (2022).

573 20 Feng, J. *et al.* A Genetically Encoded Fluorescent Sensor for Rapid and Specific In Vivo
574   Detection of Norepinephrine. *Neuron* **102**, 745-761 e748,
575   doi:10.1016/j.neuron.2019.02.037 (2019).

576 21 Conklin, B. R., Farfel, Z., Lustig, K. D., Julius, D. & Bourne, H. R. Substitution of three amino
577   acids switches receptor specificity of Gq alpha to that of Gi alpha. *Nature* **363**, 274-276,
578   doi:10.1038/363274a0 (1993).

579 22 Inoue, A. *et al.* Illuminating G-Protein-Coupling Selectivity of GPCRs. *Cell* **177**, 1933-1947
580   e1925, doi:10.1016/j.cell.2019.04.044 (2019).

581 23 Scammell, T. E., Jackson, A. C., Franks, N. P., Wisden, W. & Dauvilliers, Y. Histamine: neural
582   circuits and new medications. *Sleep* **42**, doi:10.1093/sleep/zsy183 (2019).

583 24 Inagaki, N. *et al.* Organization of histaminergic fibers in the rat brain. *J Comp Neurol* **273**,
584   283-300, doi:10.1002/cne.902730302 (1988).

585 25 Saper, C. B., Scammell, T. E. & Lu, J. Hypothalamic regulation of sleep and circadian
586   rhythms. *Nature* **437**, 1257-1263, doi:10.1038/nature04284 (2005).

587 26 Strecker, R. E. *et al.* Extracellular histamine levels in the feline preoptic/anterior
588   hypothalamic area during natural sleep-wakefulness and prolonged wakefulness: an in
589   vivo microdialysis study. *Neuroscience* **113**, 663-670, doi:10.1016/s0306-4522(02)00158-
590   6 (2002).

591 27 Chu, M. *et al.* Extracellular histamine level in the frontal cortex is positively correlated with
592   the amount of wakefulness in rats. *Neurosci Res* **49**, 417-420,
593   doi:10.1016/j.neures.2004.05.001 (2004).

594 28 Parmentier, R. *et al.* The brain H3-receptor as a novel therapeutic target for vigilance and
595   sleep-wake disorders. *Biochem Pharmacol* **73**, 1157-1171, doi:10.1016/j.bcp.2007.01.002
596   (2007).

597 29 Lohse, M. J. *et al.* Kinetics of G-protein-coupled receptor signals in intact cells. *Brit J
598   Pharmacol* **153 Suppl 1**, S125-132, doi:10.1038/sj.bjp.0707656 (2008).

599 30 Wan, J. *et al.* A genetically encoded sensor for measuring serotonin dynamics. *Nat
600   Neurosci* **24**, 746-752, doi:10.1038/s41593-021-00823-7 (2021).

601 31 Ligneau, X. *et al.* Neurochemical and behavioral effects of ciproxifan, a potent histamine
602   H3-receptor antagonist. *J Pharmacol Exp Ther* **287**, 658-666 (1998).

603 32 Gondard, E. *et al.* Enhanced histaminergic neurotransmission and sleep-wake alterations,
604   a study in histamine H3-receptor knock-out mice. *Neuropsychopharmacology* **38**, 1015-
605   1031, doi:10.1038/npp.2012.266 (2013).

606 33 Ericson, H., Watanabe, T. & Kohler, C. Morphological analysis of the tuberomammillary
607   nucleus in the rat brain: delineation of subgroups with antibody against L-histidine
608   decarboxylase as a marker. *J Comp Neurol* **263**, 1-24, doi:10.1002/cne.902630102 (1987).

609 34 Wada, H., Inagaki, N., Yamatodani, A. & Watanabe, T. Is the histaminergic neuron system
610   a regulatory center for whole-brain activity? *Trends in Neurosciences* **14**, 415-418 (1991).

611   35   Inagaki, N. *et al.* An analysis of histaminergic efferents of the tuberomammillary nucleus
612   to the medial preoptic area and inferior colliculus of the rat. *Exp Brain Res* **80**, 374-380,
613   doi:10.1007/BF00228164 (1990).
614   36   Wenkai Lin *et al.* Whole-brain mapping of histaminergic circuit in mouse brain. *Co-*
615   *submitted* (2022).
616   37   Zhou, F. M., Liang, Y. & Dani, J. A. Endogenous nicotinic cholinergic activity regulates
617   dopamine release in the striatum. *Nat Neurosci* **4**, 1224-1229, doi:10.1038/nn769 (2001).
618   38   Liu, C. *et al.* An action potential initiation mechanism in distal axons for the control of
619   dopamine release. *Science* **375**, 1378-1385, doi:10.1126/science.abn0532 (2022).
620   39   Panula, P. & Nuutinen, S. The histaminergic network in the brain: basic organization and
621   role in disease. *Nat Rev Neurosci* **14**, 472-487, doi:10.1038/nrn3526 (2013).
622   40   Ercan-Sencicek, A. G. *et al.* L-histidine decarboxylase and Tourette's syndrome. *N Engl J*
623   *Med* **362**, 1901-1908, doi:10.1056/NEJMoa0907006 (2010).
624   41   Hardie, R. C. Is histamine a neurotransmitter in insect photoreceptors? *J Comp Physiol A*
625   **161**, 201-213, doi:10.1007/BF00615241 (1987).
626   42   Hardie, R. C. A histamine-activated chloride channel involved in neurotransmission at a
627   photoreceptor synapse. *Nature* **339**, 704-706, doi:10.1038/339704a0 (1989).
628   43   Barger, Z., Frye, C. G., Liu, D., Dan, Y. & Bouchard, K. E. Robust, automated sleep scoring
629   by a compact neural network with distributional shift correction. *PLoS One* **14**, e0224642,
630   doi:10.1371/journal.pone.0224642 (2019).
631   44   Sun, F. *et al.* Next-generation GRAB sensors for monitoring dopaminergic activity in vivo.
632   *Nat Methods* **17**, 1156-1166, doi:10.1038/s41592-020-00981-9 (2020).
633

634   **Figure legends**

635   **Fig. 1: Development of genetically encoded fluorescent GRAB$_{HA}$ sensors.**

636   (a) Schematic depiction of the principle behind the GRAB$_{HA}$ sensors in which cpEGFP is

637   inserted within the receptor. Upon binding HA, the resulting conformational change causes an

638   increase in fluorescence.

639   (b) Steps used to identify the most responsive candidate HA sensors based on the human H$_4$R

640   and GRAB$_{NE}$ ICL3, by screening the ICL3 insertion sites, the ICL3 linker length, and key

641   residues in the linker and cpEGFP. Shown is the final HA1h sensor used in this study, as well

642   as the corresponding HA1mut sensor used in this study as a negative control.

643   (c) Schematic depiction of the principle used to generate and screen GRAB$_{HA}$ sensors derived

644   from other species' HA receptors.

645   (d) Further development of HA sensors by screening H1, H3, and H4 receptors obtained from

646   the indicated species.

647   (e) Optimization of candidate HA sensors based on the water bear (tardigrade) H$_1$R.

648   (f-j) Characterization of the expression and performance of the HA1h, HA1m, and HA1mut

649   sensors expressed in HEK293T cells, showing membrane trafficking (f), representative time

650   courses (g), relative brightness (h), peak response to HA (i), and apparent affinity (j). Scale bar,

651   50 μm. Data are shown as mean ± s.e.m. in h,i,j with the error bars or shaded regions indicating

652   the s.e.m., *** $P < 0.001$; n.s., not significant.

653

654

655   **Fig. 2: Characterization of GRAB$_{HA}$ sensors in HEK293T cells and cultured rat cortical**

656   **neurons.**

657   (a-c) Measurement of the kinetics of HA1h and HA1m expressed in HEK293T cells. HA was

658   applied to cells expressing either HA1h or HA1m in order to measure τ_{on}. The appropriate

659   antagonist (100 μM JNJ-7777120 for HA1h, 100 μM clemastine for HA1m) was then applied

660   in the continued presence of HA in order to measure τ_{off}. Representative traces (b) and summary

661   results (c) are shown; the white dashed line in (a) indicates the line-scanning region. $n \geq 10$

662   cells from 4-5 cultures. Scale bar, 50 μm.

663   (d and e) G protein (d) and β-arrestin (e) coupling were measured in cells expressing HA1h (or

664   H$_4$R as a positive control) or HA1m (or H$_1$R as a positive control) using Ca^{2+} imaging (d) and

665   a Tango assay (e). ** $P < 0.01$; n.s., not significant.

666   (f-i) Characterization of the expression and performance of the HA1h, HA1m, and HA1mut

667   sensors expressed in cultured rat cortical neurons, showing membrane trafficking (f),

668   representative responses (g), peak response to HA (h), and apparent affinity (i). Scale bar, 100

669   μm left panel, 20 μm right panel in f; 100 μm in g.

670   (j) Summary of the normalized fluorescence change measured in cultured rat cortical neurons

671   expressing HA1h (top panel) or HA1m (bottom panel) in response to HA alone, HA applied

672   together with the indicated HA receptor antagonist, HA precursor, metabolites, and the

673   indicated neurotransmitters (all compounds were applied at 5 μM). Clem: clemastine; Rani:

674   ranitidine; Cip: ciproxifan; JNJ: JNJ-7777120; ImAA: imidazoleacetic acid; ImPA:

675   imidazolepyruvic acid; MHTM: 1-methylhistamine; MImAA: methylimizoleacetic acid; DA:

676   dopamine; NE: norepinephrine; 5-HT: serotonin; OA: octopamine; TA: tyramine; Glu:

677   glutamate; GABA: γ-aminobutyric acid; ACh: acetylcholine; Ado: adenosine. $n = 3$ wells for

678   different groups. Paired two-tailed Student's t-tests were performed. ** $P < 0.01$; n.s., not
679   significant. Data are shown as mean ± s.e.m. in c,d,e,h,i,j with the error bars indicating the s.e.m.
680

681   **Fig. 3: Using the GRAB$_{HA}$ sensor to measure the release of endogenous HA in acute mouse**
682   **brain slices.**
683   (a) Schematic illustration of the acute mouse brain slice experiments. An AAV expressing hSyn-
684   HA1m was injected into the PFC region; acute brain slices (coronal slices containing the PFC)
685   were then prepared and used for electrical stimulation experiments.
686   (b) Exemplar 2-photon microscopy images showing HA1m expressed in the PFC. Scale bars:
687   100 μm (left) and 20 μm (right).
688   (c) Representative pseudocolor images showing the corresponding fluorescence change in
689   HA1m-expressing slices in response to 1, 10, 20, 50, and 100 pulses delivered at 20 Hz in ACSF,
690   and in response to 100 pulses in the presence of the H$_1$R antagonist clemastine (20 μM). Scale
691   bar, 100 μm.
692   (d) Exemplar traces (left) and summary of the peak fluorescence change (right) measured in
693   HA1m-expressing slices stimulated as indicated. Where indicated, clemastine was applied at
694   20 μM. *** $P < 0.001$.
695   (e) Representative trace with fitted curves (left) and summary data of the on-time and off time
696   constants (right) measured for the change in HA1m fluorescence in response to the indicated
697   number of pulses applied at 20 Hz.
698   (f) Exemplar time-lapse pseudocolor images of HA1m fluorescence in response to 100 pulses
699   at 20 Hz applied during the first 5 s. Scale bar, 100 μm
700   (g) Spatial profile of the evoked change in fluorescence shown in panel (f); the vertical dashed
701   line at time 0 indicates the start of the stimulation.
702   (h) Temporal dynamics of the change in HA1m fluorescence as shown in (g) measured 10, 20,
703   50, and 100 μm from the release center.
704   (i) Spatial dynamics of the change in HA1m fluorescence as shown in (g) measured 3, 5, 10,
705   and 30 s after the onset of stimulation. Each curve was fitted with a Gaussian function.
706   (j) Left, a representative diffusion coefficient was measured by plotting the square of the full
707   width at half maximum (FWHM) against time based on the data show in (i). Right, summary
708   of the diffusion coefficients measured from the data shown in (i). Data are shown as mean ±
709   s.e.m. in d,e,j with the error bars indicating the s.e.m.
710

711   **Fig. 4: Using the GRAB$_{HA1m}$ sensor to measure *in vivo* HA release in the POA during the**
712   **sleep-wake cycle in freely moving mice.**
713   (a) Schematic diagram depicting the strategy for fiber photometry recording of HA1m
714   fluorescence in the preoptic area (POA) of freely behaving wild-type (WT) and histidine
715   decarboxylase knockout (HDC KO) mice during the sleep-wake cycle. Top panel, an AAV
716   expressing hSyn-HA1m was injected into the PFC region; middle panel, schematic diagram
717   depicting fiber photometry recording of HA1m signals, EEG, and EMG. Bottom panel, HA
718   synthesis process.
719   (b and d) Example traces of simultaneous EEG, EMG, and HA1m recordings in a WT (b) and
720   HDC KO (d) mouse. In this and subsequent figures, the wake state is shaded in blue, REM
721   sleep is shaded in pink, and NREM sleep is unshaded.

722   (c and e) Summary of the average HA1m fluorescence measured in WT (c; n=6 mice) and HDC
723   KO mice (e; n = 5 mice) in the indicated sleep-wake states. Each symbol represents the
724   recording from one mouse. (c) One-way ANOVA: F = 16.3913, P = 0.0007; Tukey's *post hoc*
725   test: Wake vs NREM P = 0.0335, Wake vs REM P = 0.0207, NREM vs REM P = 0.0153; * P
726   < 0.05. (e) One-way ANOVA: F = 1.2401, P = 0.3308; n.s., not significant.
727   (f) Time course and average signals measured for the HA1m sensor during the indicated
728   transitions between sleep-wake states. The vertical dashed lines at time 0 represent the
729   transition time. paired t-test, REM→Wake t = 4.2803, P = 0.0079; NREM→Wake t = 4.0586,
730   P = 0.0097; Wake→NREM t = 3.7418, P = 0.0134; NREM→REM t = 3.9835, P = 0.0105; *
731   P < 0.05, ** P < 0.01. Data are shown as mean ± s.e.m. in c,e,f with the error bars or shaded
732   regions indicating the s.e.m. in f, the shaded lines indicating the mean trace of individual mice.
733

734   **Fig. 5: Using the GRAB$_{HA}$ sensor to measure HA release in the PFC in freely moving mice**
735   **during the sleep-wake cycle.**
736   (a) Schematic diagram depicting the strategy for fiber photometry recording of HA1h or
737   HA1mut fluorescence in the prefrontal cortex (PFC) of freely behaving mice during the sleep-
738   wake cycle. Top panel, an AAV expressing either HA1h or HA1mut was injected into the PFC
739   region, and an optical fiber was implanted at the injection site. Bottom three panels, schematic
740   diagram showing the responses the HA1h and HA1mut sensors to HA, as well as the HA1h
741   sensor in the presence of an H$_4$R antagonist.
742   (b and f) Example traces of simultaneous EEG, EMG, and HA1h (b) or HA1mut (d) recordings.
743   (c and g) Summary of the average HA1h (c) and HA1mut (e) fluorescence responses measured
744   in the indicated sleep-wake states; (c) n = 9 mice. One-way ANOVA: F = 21.7374, P = 0.0014;
745   Tukey's *post hoc* test: Wake vs NREM P = 0.0074, Wake vs REM P = 0.0033, NREM vs REM
746   P = 0.0011; ** P < 0.01. (e) n = 4 mice. One-way ANOVA: F = 9.5591, P = 0.0512; n.s., not
747   significant.
748   (d) Example traces of simultaneous EEG, EMG, and HA1h recordings after an i.p. injection of
749   the H$_4$R antagonist JNJ-7777120 (3 mg/kg body weight).
750   (e) Summary of average HA1h fluorescence measured before (Pre) and after (Post) an injection
751   of JNJ-7777120. n = 8 mice Paired t-test, t = 6.3859, P = 0.0004; ** P < 0.01.
752   (h) Schematic drawing depicting the effect of the H$_3$R antagonist ciproxifan on downstream HA
753   release.
754   (i) Example traces of simultaneous EEG, EMG, and HA1h recordings in mice before and after
755   administration of vehicle, ciproxifan (3 mg/kg body weight), or caffeine (15 mg/kg body
756   weight).
757   (j) Time course of the probability of being in the awake state; the dashed line at time 0 indicates
758   the administration of vehicle, ciproxifan, or caffeine.
759   (k) Time course (left) and average HA1h signals (right) measured in the PFC before and after
760   administration of vehicle, ciproxifan, or caffeine. n = 8. Two-way ANOVA between brain state
761   and time; Vehicle, F(time) = 3.9317, P = 0.0878; Ciproxifan, F(time) = 57.1062, P = 0.0001,
762   pre-post comparisons followed by Sidak's test, Wake, NREM, and REM pre vs post P < 0.0001;
763   caffeine, F(time) = 0.1526, P = 0.7076; ** P < 0.01. n.s., not significant. Data are shown as
764   mean ± s.e.m. in c,e,g,j,k with the error bars or shaded regions indicating the s.e.m.
765

766 **Fig. 6: Simultaneously recording HA release in the mouse PFC and POA during the sleep-**
767 **wake cycle reveals differences in kinetics.**
768 (a) Schematic diagram depicting the strategy for simultaneously recording HA1h fluorescence
769 in the PFC and POA during the sleep-wake cycle in a freely moving mouse.
770 (b) Example traces of simultaneous EEG, EMG, and HA1h recordings in the PFC and POA.
771 (c) Summary of average HA1h fluorescence measured in the in the POA and PFC during the
772 indicated sleep-wake states; $n = 5$ mice. Two-way ANOVA between brain state and nuclei,
773 F(brain state) $= 20.4065$, $P = 0.0007$; F(nuclei) $= 0.4091$, $P = 0.5572$. n.s., not significant.
774 (d) Cross-correlation between the HA1h signals measured in the POA and PFC; as a control,
775 the data were also shuffled and depicted as the horizontal line at $y=0$. $n = 5$ mice.
776 (e) Time courses of the change in HA1h fluorescence measured in the POA and PFC at the
777 indicated transitions between sleep-wake states. The vertical dashed lines represent the
778 transition time.
779 (f) Summary of t_{50} measured for the change in HA1h fluorescence in the POA and PFC during
780 the indicated sleep-wake state transitions. $n = 5$ mice. Two-way ANOVA between brain state
781 transition and nuclei followed by Sidak's test, F(nuclei) $= 52.4873$, $P = 0.0020$. REM→Wake,
782 $P = 0.0156$; NREM→Wake, $P < 0.0001$; Wake→NREM, $P = 0.0006$; NREM→REM, $P = 0.996$;
783 * $P < 0.05$, ** $P < 0.01$.
784 (g) Summary of the dynamics measured in the POA and PFC at the transitions between the
785 various sleep-wake states.
786 Data are shown as mean $\pm$ s.e.m. in c,d,e,f with the error bars or shaded regions indicating the
787 s.e.m.
788
789 **Supplementary Fig. 1: Screening of HA sensors with good membrane trafficking from**
790 **four human HA receptors**
791 (a) Summary of the reported EC50 values for the indicated human HA receptors (source:
792 https://www.guidetopharmacology.org/).
793 (b) Analysis of fluorescence and membrane trafficking of all four human HA receptors
794 containing cpEGFP expressed in HEK293T cells; membrane-targeted RFP (RFP-CAAX) was
795 co-expressed to label the plasma membrane. Left, fluorescence images of HEK293T cells
796 expressing the indicated HA receptor-based chimeras (green) and RFP (red). Middle,
797 normalized line-scanning plots of the fluorescence signals measured in both the green and red
798 channels. Right, summary of Pearson's co-localization ratio measured between the indicated
799 HA receptor-based chimeras and RFP-CAAX; *** $P < 0.001$ versus hH4R. Scale bar, 20 μm.
800
801 **Supplementary Fig. 2: The amino acid sequences of the GRAB$_{HA}$ sensors.**
802 The amino acid sequences of the GRAB$_{HA1h}$ (a) and GRAB$_{HA1m}$ (b) sensors are shown, with
803 the indicated domains shown above. Also shown is the location of the E211A mutation (blue
804 arrowhead) in GRAB$_{HA1h}$ to generate the GRAB$_{HA1mut}$ sensor.
805
806 **Supplementary Fig. 3: Characterization of the wavelength spectra and specificity of HA**
807 **sensors expressed in HEK293T cells**
808 (a) One-photon excitation (Ex) and emission (Em) spectra (left) and two-photon excitation
809 spectra (right) of HA1h and HA1m measured in the absence and presence of HA.

810 (b) Summary of the normalized change in fluorescence measured for HA1h (top panel) and
811 HA1m (bottom panel) expressed in HEK293T cells in response to the indicated compounds
812 (applied at 5 μM each); see Fig. 2 for abbreviations. n = 3 wells for different groups. Paired
813 two-tailed Student's t-tests were performed. *** $P < 0.001$; n.s., not significant.

814

815 **Supplementary Fig. 4: 3-h recording of HA1h and HA1m expressed in cultured cortical**
816 **neurons.**
817 Shown are fluorescence images (a) and summary data (b) of the indicated HA sensors expressed
818 in cultured neurons before (Pre) and during a 3-h application of HA at saturating concentration,
819 followed by application of the corresponding antagonist.

820

821 **Supplementary Fig. 5: [³H]HA radioligand binding assay for HA1h sensor.**
822 (a) Binding affinity measurement. Specific binding of increasing concentrations [³H]HA to
823 HEK293T cell homogenates expressing HA1h, HA1mut, or H_4R. TB: total binding, NSB:
824 nonspecific binding.
825 (b) [³H]HA radioligand competition binding assay for measurement of [³H]HA (8.5 nM)
826 binding to test whether HA, H_4R agonist, HA precursor, HA metabolites, and other
827 monoamines, neurotransmitters, and chemicals (all compounds were applied at 30 μM) bind
828 to HA1h sensor (top panel) and WT H_4R (bottom panel).

829

830

831 **Supplementary Fig. 6: Wake-promoting agent, H_3R antagonist, enhanced HA level in the**
832 **PFC of mice, extend shown time in Fig. 5i,j,k.**
833 (a) Typical traces of EEG, EMG and HA1h signals after administration of wake-promoting
834 agents, H3R antagonist, ciproxifan at 3 mg/kg, or caffeine at 15 mg/kg, or vehicle in WT
835 mice, extend shown time in Fig. 5i.
836 (b) Time courses of wake probability before and after administration of ciproxifan, caffeine
837 and vehicle, extend shown time in Fig. 5j.
838 (c) Time courses of HA1h signals before and after administration of ciproxifan, caffeine and
839 vehicle, extend shown time in Fig. 5k.
840 (d) Typical traces of EEG, EMG and HA1m signals after administration of H3R antagonist,
841 ciproxifan at 3 mg/kg in WT mouse (left panel) and HDC KO mouse (right panel).
842 (e) Time courses of HA1m signals before and after administration of ciproxifan in WT mouse
843 and HDC KO mouse.
844 (f) Ground data of HA1m signals before and after administration of ciproxifan in WT mouse
845 and HDC KO mouse. Two-way ANOVA between genotype and time; F(time) = 9.6457, P =
846 0.0267, pre-post comparisons followed by Sidak's test WT pre vs post $P = 0.0107$, HDC KO
847 pre vs post $P = 0.9989$;

848

849

850 **Supplementary Fig. 7 HA1h can be used to measure HA dynamics over one day *in vivo*.**
851 (a) Schematic diagram depicting Simultaneous recording of HA1h in the PFC and POA
852 during sleep–wake cycles.
853 (b) Typical traces of EEG, EMG and HA1h signals over 24h. The brain states are color-coded.

854   (c)Summary data of first and last hour averaged HA1h signals. Paired two-tailed Student's t-

855   tests were performed. $t = 2.184$, $P = 0.161$. n.s., not significant.

856

857   **Supplementary Fig.8: Model depicting two possible explanations for the difference in**
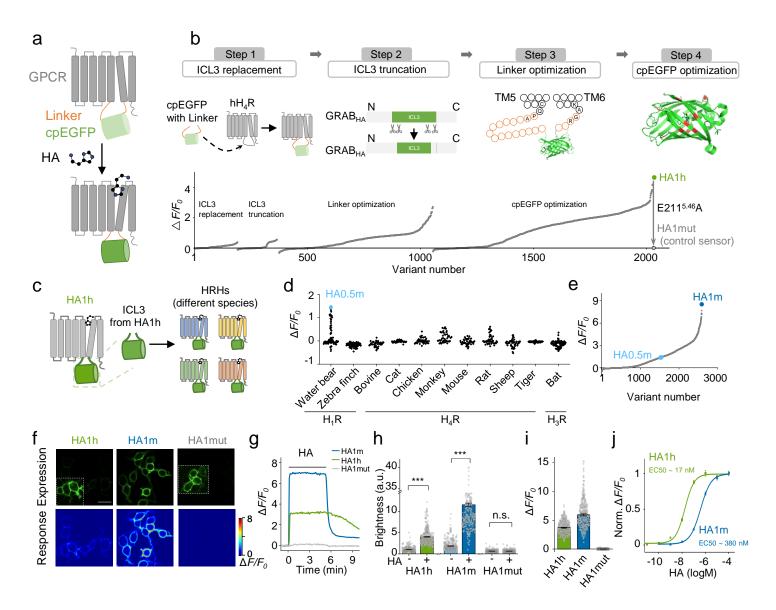
858   **HA release kinetics between the POA and PFC.**

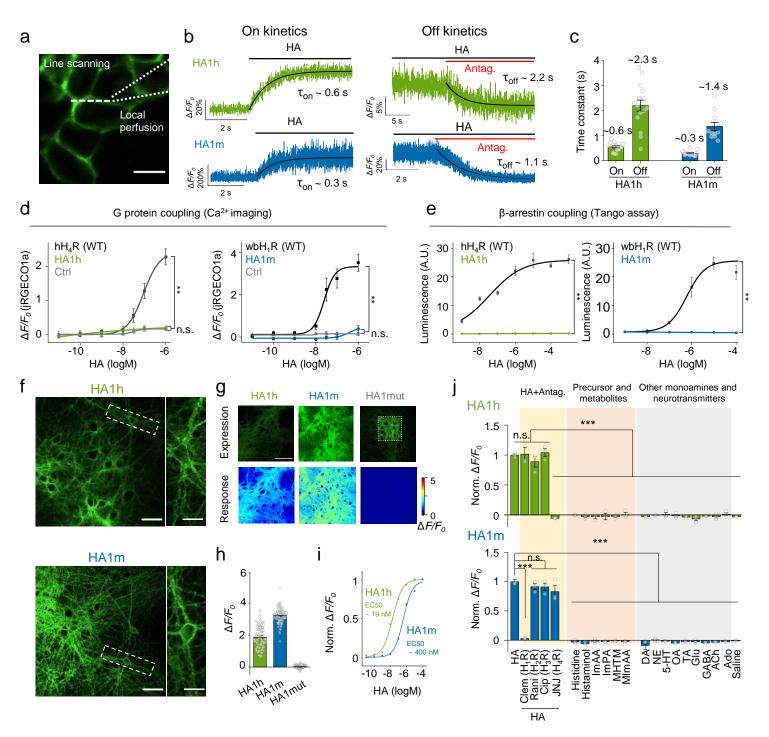**Fig. 1 Development of genetically encoded fluorescent GRAB_HA sensors**

Fig. 2 Characterization of GRAB$_{HA}$ sensors in HEK293T cells and cultured rat cortical neurons.
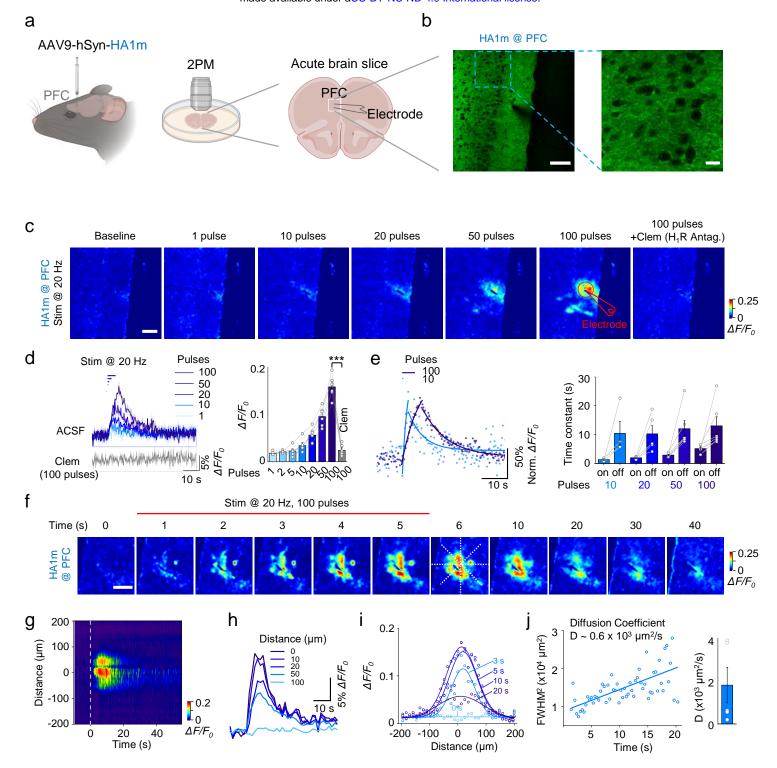
Fig. 3 Using the GRAB_HA sensor to measure the release of endogenous HA in acute mouse brain slices
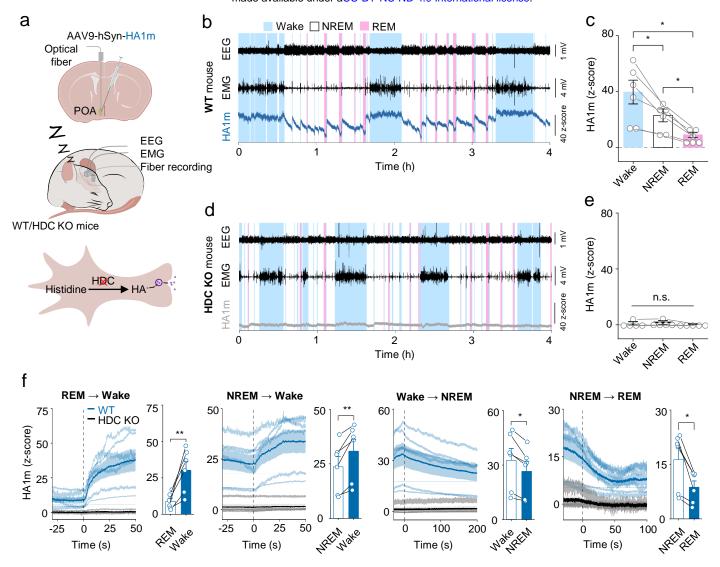
Fig. 4 Using the GRAB$_{HA1m}$ sensor to measure *in vivo* HA release in the POA during the sleep-wake cycle in freely moving mice
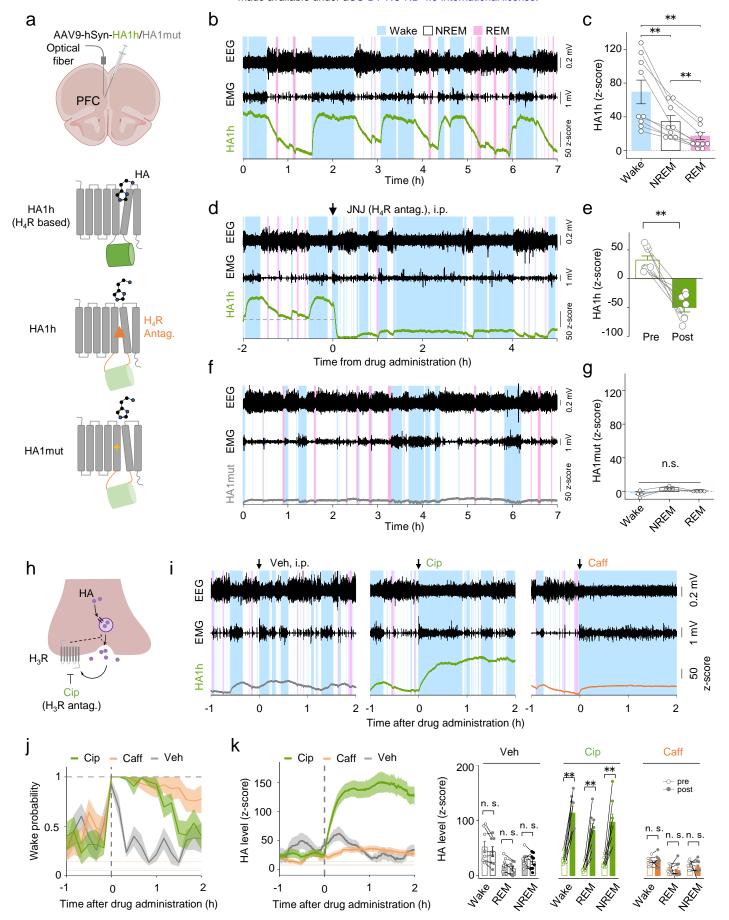
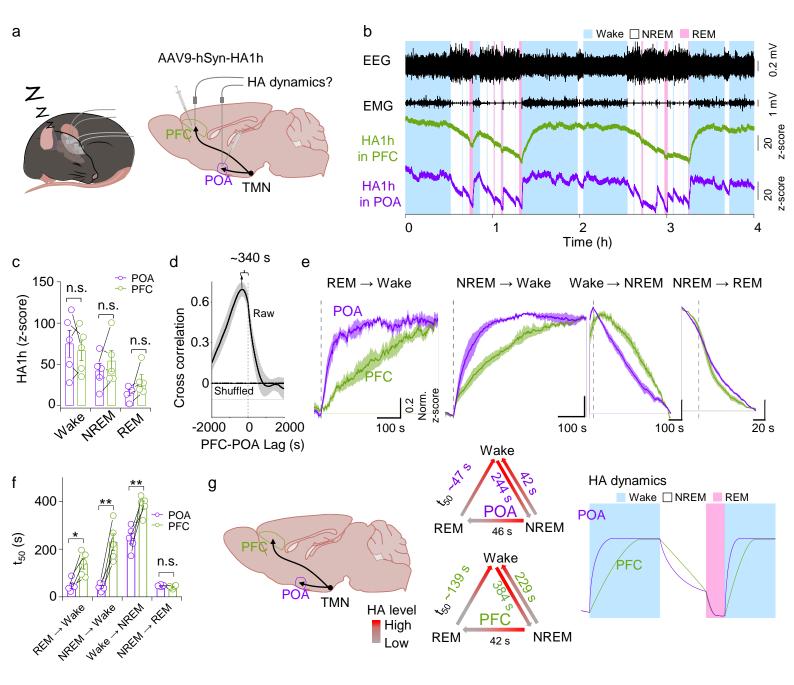**Fig. 5 Using the GRAB$_{HA1h}$ sensor to measure HA release in the PFC in freely moving mice during the sleep-wake cycle**
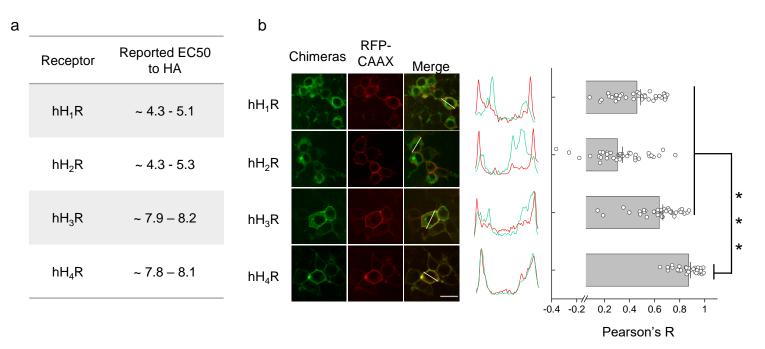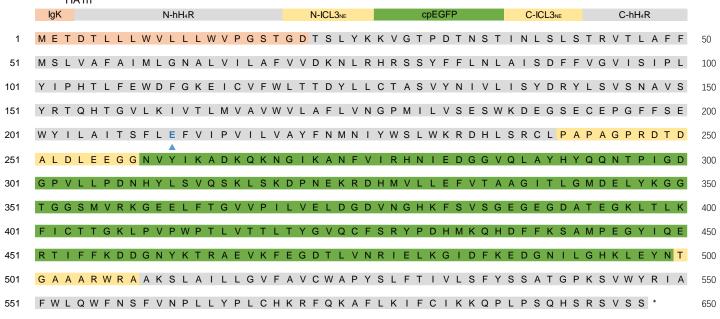
Fig. 6 Simultaneously recording HA release in the mouse PFC and POA during the sleep-wake cycle reveals differences in kinetics

a

Receptor	Reported EC50 to HA
hH$_1$R	~ 4.3 - 5.1
hH$_2$R	~ 4.3 - 5.3
hH$_3$R	~ 7.9 – 8.2
hH$_4$R	~ 7.8 – 8.1

b

Supplementary Fig. 1 Screening of HA sensors with good membrane trafficking from four human HA receptors
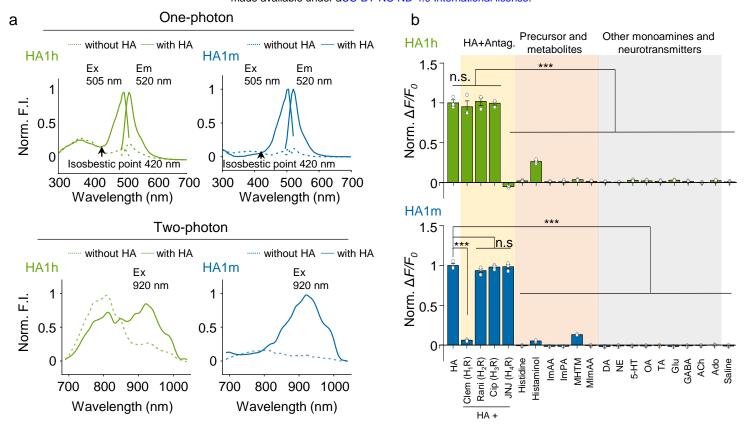
a

GRAB$_{HA1h}$

| IgK | N-hH₄R | N-ICL3$_{NE}$ | cpEGFP | C-ICL3$_{NE}$ | C-hH₄R |

```
  1  M E T D T L L L W V L L L W V P G S T G D T S L Y K K V G T P D T N S T I N L S L S T R V T L A F F  50
 51  M S L V A F A I M L G N A L V I L A F V V D K N L R H S S Y F F L N L A I S D F F V G V I S I P L  100
101  Y I P H T L F E W D F G K E I C V F W L T T D Y L L C T A S V Y N I V L I S Y D R Y L S V S N A V S  150
151  Y R T Q H T G V L K I V T L M V A V W W L A F L V N G P M I L V S E S W K D E G S E C E P G F F S E  200
201  W Y I L A I T S F L E F V I P V I L V A Y F N M N I Y W S L W K R D H L S R C L P A P A G P R D T D  250
251  A L D L E E G G N V Y I K A D K Q K N G I K A N F V I R H N I E D G G V Q L A Y H Y Q Q N T P I G D  300
301  G P V L L P D N H Y L S V Q S K L S K D P N E K R D H M V L L E F V T A A G I T L G M D E L Y K G G  350
351  T G G S M V R K G E E L F T G V V P I L V E L D G D V N G H K F S V S G E G E G D A T E G K L T L K  400
401  F I C T T G K L P V P W P T L V T T L T Y G V Q C F S R Y P D H M K Q H D F F K S A M P E G Y I Q E  450
451  R T I F F K D D G N Y K T R A E V K F E G D T L V N R I E L K G I D F K E D G N I L G H K L E Y N T  500
501  G A A A R W R A A K S L A I L L G V F A V C W A P Y S L F T I V L S F Y S S A T G P K S V W Y R I A  550
551  F W L Q W F N S F V N P L L Y P L C H K R F Q K A F L K I F C I K K Q P L P S Q H S R S V S S *  650
```

HA1mut site: E211$^{5.46}$A

b

GRAB$_{HA1m}$

| IgK | N-wbH₁R | N-ICL3$_{NE}$ | cpEGFP | C-ICL3$_{NE}$ | C-wbH₁R |

```
  1  M E T D T L L L W V L L L W V P G S T G D T S L Y K K V G T T G M E P A G A G G A A I L L D D D D D  50
 51  Y Y L T T P G Y P G S G S N A S L S P P A D L F P A A S N H S T A V V V S G D L D L Y V I I P L G I  100
101  F L A V L S L V T F A G N V M V L H A L R T E K K L Q T V S N I F I M S L A I A D C S V G L F A M P  150
151  L S A V Y A L L G Y W P F G L V V C N M W L S M D Y V A S T A S I F N L F A L S L D R F W S I I S P  200
201  L R Y L K K R T R K R A I I M C S S V W L A S L L W I I P V V G W H Q M F N D G R R D V P V E E C D  250
251  T E F A D E Q V F K V L T A I F N F Y V P M A A M I A L Y G R I F H E I K L R A A S Q P A P A G P R  300
301  D T D A L D L E E G G N V Y I K A D K Q K N G I K A N F V I R H N I E D G G V Q L A Y H Y Q Q N T P  350
351  I G D G P V L L P D N H Y L S V Q S K L S K D P N E K R D H M V L L E F V T A A G I T L G M D E L Y  400
401  K G G T G G S M V R K G E E L F T G V V P I L V E L D G D V N G H K F S V S G E G E G D A T E G K L  450
451  T L K F I C T T G K L P V P W P T L V T T L T Y G V Q C F S R Y P D H M K Q H D F F K S A M P E G Y  500
501  I Q E R T I F F K D D G N Y K T R A E V K F E G D T L V N R I E L K G I D F K E D G N I L G H K L E  550
551  Y N T G A A A R W R A K K A A F Q L G V I L G A F C L C F M P Y F I S F I I T A F C K D C V S P A V  650
601  H S I F T W L G Y V N S T T N P F L Y T W T N A N F R S A F R K I L R M K E T P K K P V Y M Q M P H  700
651  K T P R P K K Q P L E A R V S G T A S G G T T A P A R K S D D T R L *  750
```
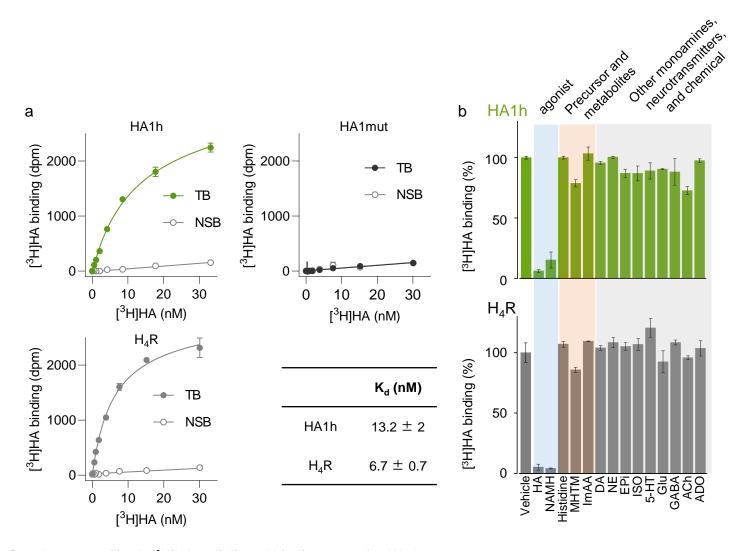
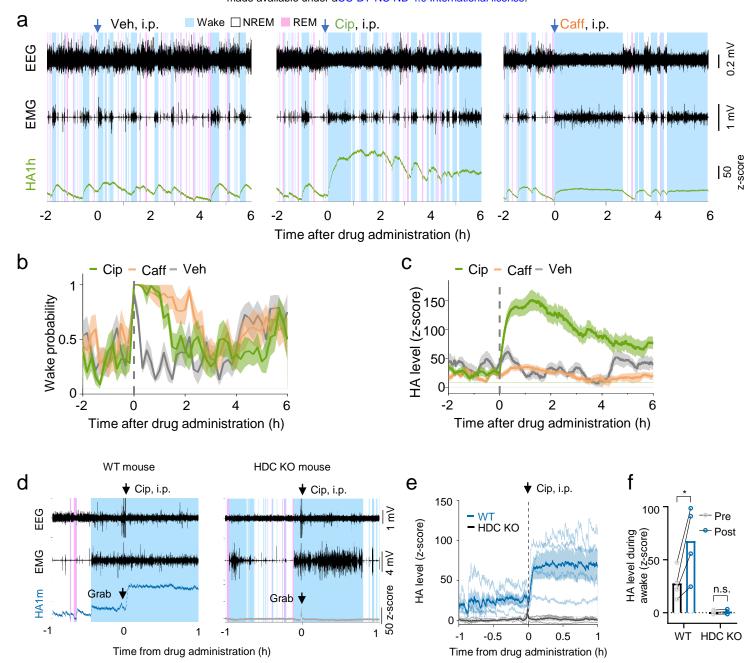**Supplementary Fig. 2 The full amino acid sequences of the GRAB$_{HA}$ sensors**

Supplementary Fig. 3 Characterization of the wavelength spectra and specificity of HA sensors expressed in HEK293T cells
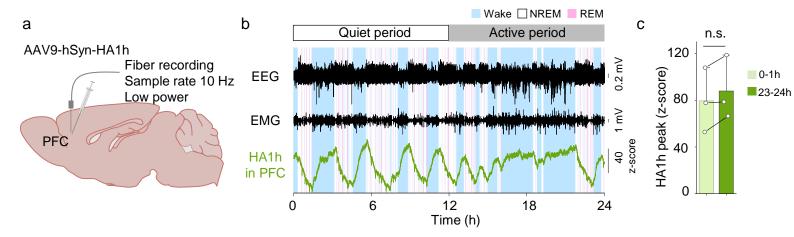
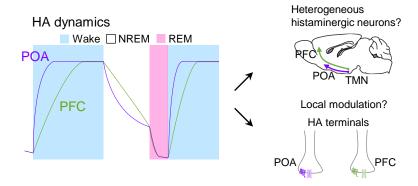**Supplementary Fig. 4 3-h recording of HA1h and HA1m expressed in cultured cortical neurons.**

Supplementary Fig. 5: [³H]HA radioligand binding assay for HA1h sensor

Supplementary Fig. 6 Wake-promoting agent, H$_3$R antagonist, enhanced HA level in the PFC of mice, extend shown time in Fig. 5i, j, k.

Supplementary Fig. 7 HA1h can be used to measure HA dynamics over one day *in vivo*

Supplementary Fig. 8 Model depicting two possible explanations for the difference in HA release kinetics between the POA and PFC.